Mechanical Systems and Signal Processing 156 (2021) 107629

Contents lists available at ScienceDirect

Mechanical Systems and Signal Processing

journal homepage: www.elsevier.com/locate/ymssp

Dynamic characterization of a system with degradation: A masonry wall

C. Gatta, F. Vestroni *, D. Addessi

Department of Structural and Geotechnical Engineering, Sapienza University of Rome, Via Eudossiana 18, 00184 Rome, Italy

ARTICLE INFO

Article history:
Received 6 September 2020
Received in revised form 19 December 2020
Accepted 9 January 2021
Available online 3 February 2021

2010 MSC:
00-01
99-00

Keywords:
Frequency response curves
Degrading systems
Masonry wall
Dynamic response
Experimental tests

ABSTRACT

Characterization of the dynamic behavior of linear systems is exhaustively described with a single frequency response curve (*frc*). For nonlinear systems, which tend to depend on load amplitude, at least one *frc* for each excitation intensity is required to detect the main characteristics of the dynamic response. Nonlinear systems, more commonly dealt with in the literature, are invariant with respect to the deformation history and, thus, *frcs* obtained with increasing and decreasing driving frequency coincide, apart from the frequency range with coexistent solutions. This is not so for many real systems which suffer from their past, often exhibiting degradation of their mechanical properties. Here the focus is on the effects of damage on the dynamic signature of systems. The response of a masonry wall, representative of systems with a degrading restoring force, is analyzed under harmonic excitation. A refined finite element model is used to represent the typical degradation that occurs in masonry and its reliability is proved by comparing numerical results and experimental outcomes from shaking table tests. Particular attention is paid to the wall *frcs*, emphasizing the influence of the deformation history on the curves characteristics and their role in the dynamic characterization of a system with degradation.

1. Introduction

A single frequency response curve (*frc*) is sufficient to represent the dynamic behavior of linear systems. However, additional information is required for nonlinearity, typical of many real systems, to account for the dependency of the system response on the oscillation amplitude. Hence, focusing on the steady-state response to harmonic excitations, at least one *frc* for each forcing intensity is necessary to describe the dynamic behavior as, differently from linear systems, knowing the response to a given excitation does not predict that to same excitation with a different intensity.

Attempts have been made to extend the *frcs* of mechanical systems in the nonlinear range, by resorting to numerical studies [1–5], and sometimes along with experimental tests [1,6–8]. It emerged that the main features of *frcs* depend on the shape of the system restoring force. Although a wide variety of restoring force relationships have been proposed to describe the nonlinear behavior of materials and elements, and while these notably modify the response, few qualitative differences can be detected in terms of *frcs*. Indeed, the *frcs* can be grouped in two large families: the first includes single-valued curves (Fig. 1(a)), the latter multi-valued curves exhibiting limited frequency ranges of multiple solutions (Fig. 1(b,c)), typical of softening (Fig. 1(b)) or hardening (Fig. 1(c)) polynomial nonlinearities.

* Corresponding author.
E-mail address: vestroni@uniroma1.it (F. Vestroni).

https://doi.org/10.1016/j.ymssp.2021.107629
0888-3270/

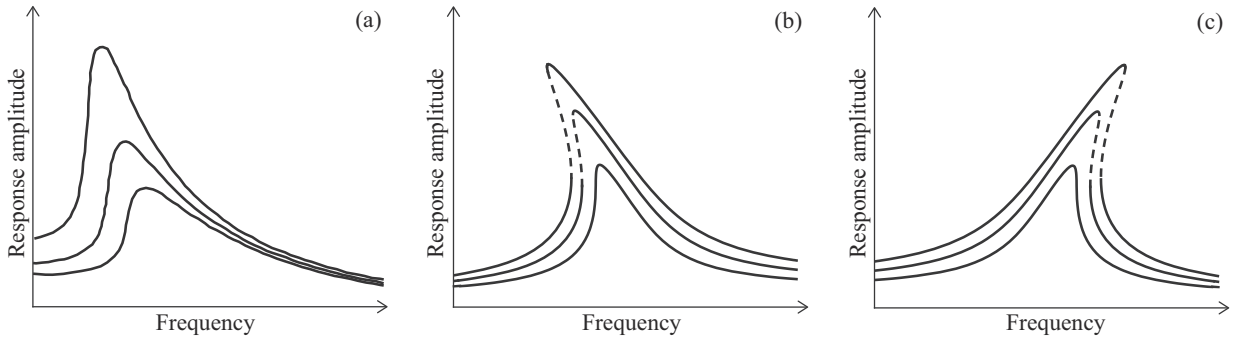

Fig. 1. (a) Single-valued and multi-valued *frcs* with (b) softening and (c) hardening behavior. Dashed lines represent unstable solutions.

Similar results are also obtained when material nonlinearity is considered, again depending on the main characteristics of the restoring force. For instance, Fig. 2 shows the *frcs* of a hysteretic single-degree-of-freedom system described by the Bouc-Wen model, which can represent general classes of hysteretic nonlinearities. In particular, instances of full and reduced hysteresis are reported. These correspond to hysteretic loops with high and reduced energy dissipation [9,10], as shown in Fig. 2 (a) by the black and red force–displacement curves. In the former case (full hysteresis) the *frc* is always single-valued (Fig. 2 (b)), whereas in the latter (reduced hysteresis) a range of coexisting solutions appears (Fig. 2(c)) [9,11–14].

The outcomes of the restoring force shape are more evident on higher order features, such as unstable branches, wrinkles, detached *frcs*, chaos [15,16], but these are beyond the scope of this study.

The signature of *frcs* and their backbone curve has been little discussed. By those who did, they were seen as a fundamental step for a more in-depth analysis of the dynamic response of nonlinear systems [17,18]. Some distinctive properties in the dynamic characterization of complex nonlinear systems were emphasized. However, focus was mainly on systems with history independent restoring force relationships, which are not affected by damage phenomena associated with the deformation process. Below, such systems will be simply denoted as invariant systems. Most constitutive laws accounting for material nonlinearity, significantly depend on the loading history, as the deformation process induces variations in the system mechanical characteristics [19,20]. This occurs when a certain level of damage considerably modifies these properties, without preventing the stabilization of the oscillation amplitude under a stationary process with a limited number of cycles.

Hence, this study focuses on the characterization of the dynamic behavior of a real case of a degrading system, that is a slender masonry wall previously analyzed by the authors [21,22]. This model can reliably pinpoint the effects of degrading mechanisms on the fundamental dynamic signature of systems. Indeed, under typical loading conditions, masonry undergoes damaging processes involving microvoids and microfractures with a significant decay of the overall stiffness and strength properties. To be noted is that in [22] the attention was mainly focused on static and cyclic response of masonry walls, using experimental results available in the literature for comparison. Here, the focus has been moved to characterize the dynamic response and ad hoc experiments are developed to validate the numerical model. The main aim is to investigate the modifications of the *frcs* due to damage, and more generally, evaluate the information on the dynamic characterization provided by *frcs*.

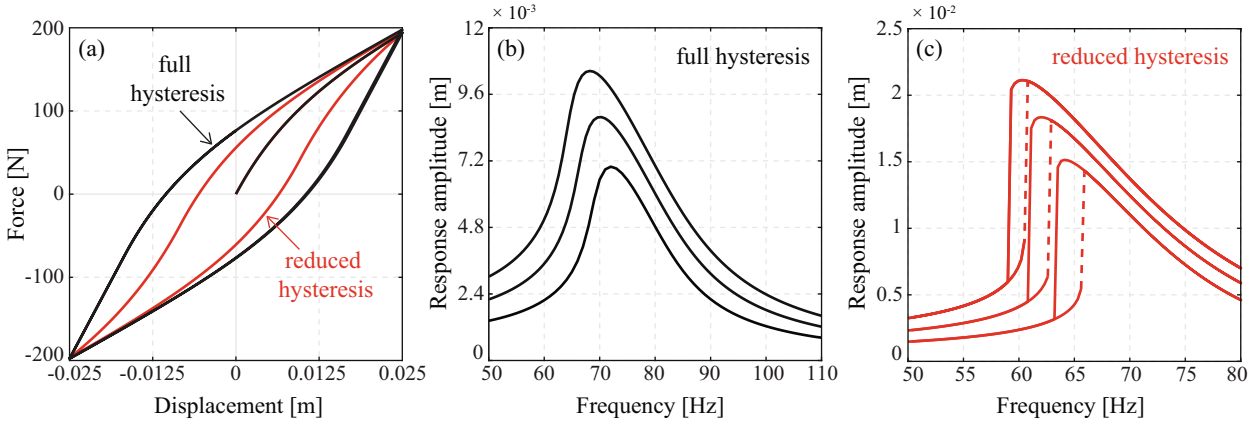

Fig. 2. Bouc-Wen model: (a) force–displacement curves with full (black curve) and reduced (red curve) hysteresis leading to (b) single-valued and (c) multi-valued *frcs*. (For interpretation of the references to colour in this figure legend, the reader is referred to the web version of this article.)

Among the available modeling strategies for masonry [23], here the macromechanical approach is adopted, with the real heterogeneous material substituted by a fictitious homogenized medium. The constitutive response is described by a phenomenological law based on a damage-plastic model. This describes strength-stiffness decay and hysteretic dissipation characterizing masonry response beyond the elastic range. Moreover, two independent damage variables, distinguished for tension and compression, are introduced to simulate the stiffness recovery due to the crack re-closure, typical of the cyclic response of quasi-brittle materials [24,25]. The model, whose reliability is proved by experimental shaking table tests, is used to describe the wall response under monotonic and cyclic loads, thus obtaining a generalized force–displacement relationship of the system with degrading properties. Then, the *frcs* are investigated, with the final goal of ascertaining the extent to which the original signature of the curves remains meaningful in representing the dynamics of systems with degrading characteristics.

2. Material and structure models

2.1. Material model

The damage-plastic model recently presented in [22] is used to describe the typical degrading and hysteresis mechanisms characterizing masonry response. First, the model fundamental equations are briefly recalled.

The heterogeneous masonry material, composed of blocks/bricks connected with mortar layers, is modeled as a fictitious homogenized medium, resorting to a macromechanical approach. Hence, the phenomenological constitutive law described in [22], based on a two-parameter isotropic damage model and a classical Von Mises plasticity formulation, is adopted to capture the following nonlinear phenomena:

- strength-stiffness decay due to onset and propagation of microcracks;
- accumulation of plastic strains caused by frictional mechanisms at brick–mortar interface;
- stiffness recovery at the crack re-closure.

Based on the damage mechanics equivalence energy principle, the relationship between stresses, $\boldsymbol{\sigma} = \{\sigma_1\, \sigma_2\, \tau_{12}\}^T$, and strains, $\boldsymbol{\varepsilon} = \{\varepsilon_1\, \varepsilon_2\, \gamma_{12}\}^T$, is defined as:

$$\boldsymbol{\sigma} = [(1 - D_t)\alpha_t + (1 - D_c)\alpha_c]^2 \mathbf{C}(\boldsymbol{\varepsilon} - \boldsymbol{\varepsilon}^p) \tag{1}$$

being $\boldsymbol{\varepsilon}^p$ the plastic strain vector and $\mathbf{C}$ the elastic constitutive matrix for plane stress condition depending on Young's modulus E and Poisson ratio ν. In Eq. (1), α_t and α_c, defined later, are two weighting coefficients ruling the combined effect of the damage variable in tension, D_t, and in compression, D_c. According to their physical meaning, D_t and D_c can vary between 0 and 1, representing the undamaged material and the fully degraded state, respectively. Furthermore, the damage variables have to satisfy the thermodynamic irreversibility condition, that is $\dot{D}_t \geqslant 0$ and $\dot{D}_c \geqslant 0$, together with the condition $D_t \geqslant D_c$. To drive the onset and evolution of damage parameters, two associated variables, Y_t and Y_c, are introduced and defined as:

$$Y_t = \sqrt{\sum_{i=1}^{3} \langle e_i \rangle_+^2} \qquad Y_c = \sqrt{\sum_{i=1}^{3} \langle e_i \rangle_-^2} \tag{2}$$

where the brackets $\langle \bullet \rangle_{+/-}$ select the positive/negative part of the quantity and e_i is the equivalent strain measure determined on the basis of the principal total strains, $\hat{\varepsilon}_i$, and the Poisson coefficient, ν, as:

$$e_i = (1 - 2\nu)\hat{\varepsilon}_i + \nu \sum_{j=1}^{3} \hat{\varepsilon}_j \tag{3}$$

Tensile, F_t, and compressive, F_c, limit functions are considered to govern the evolution of the damage variables:

$$\begin{aligned} F_t &= (Y_t - Y_{t0}) - D_t(a_t Y_t + b_t) \\ F_c &= (Y_c - Y_{c0}) - D_c(a_c Y_c + b_c) \end{aligned} \tag{4}$$

being $Y_{t0/c0}$ the initial damage thresholds ruling the onset of the damaging processes, $b_{t/c}$ and $a_{t/c}$ parameters affecting the peak strengths and the slope of the descending post-peak branches, respectively [22].

To rule the combined effect of D_t and D_c, the weighting coefficients α_t and α_c introduced in Eq. (1) are defined as:

$$\alpha_t = \frac{Y_t^e / Y_{t0}}{Y_t^e / Y_{t0} + Y_c^e / Y_{c0}} \qquad \alpha_c = 1 - \alpha_t \tag{5}$$

where $Y_{t/c}^e$ is evaluated according to Eq. (2) but on the basis of the principal elastic strains $\hat{\varepsilon}_i^e$. By the introduction of two different damage parameters and their weighting coefficients, the cyclic response of quasi-brittle materials, such as masonry, can be described. Indeed, a stiffness recovery occurs due to the re-closure of tensile cracks when the material undergoes compressive states. This phenomenon, known as the unilateral effect, justifies the imposed constraint $D_t \geqslant D_c$, which

ensures that the recovery of stiffness occurs only in the transition from tensile to compressive states. Regarding the plasticity model, a classical Von Mises formulation for a plane stress problem with linear kinematic hardening is adopted [26]. Hence, in what follows, σ_y and H_k denote the yield stress and kinematic hardening modulus, respectively.

The described constitutive model is implemented into a quadrilateral isoparametric finite element in the FEAP code [27]. The mesh-dependency numerical issues, typical of strain-softening response, are overcome by introducing the nonlocal integral regularization technique [28]. Thus, in Eqs. (4) and (5) the integral definition of the damage associated variables is adopted, depending on the selected nonlocal radius l_c accounting for the characteristic length of the microstructure and mesh size.

2.2. Structure model

The structural response of a masonry wall to monotonic and cyclic loads is analyzed. The aim is to identify the parameters of the model so that it can reliably represent degrading phenomena with respect to the other widely used models with invariant restoring forces.

The wall, already studied by the authors in [22], is characterized by height $H = 6000$ mm, width $W = 1000$ mm and thickness $t = 1000$ mm. This is representative of a strip composing a long wall loaded out-of-plane. A $2D$ model of the panel, with a mesh made of (3×19) 9-node bi-quadratic finite elements (FEs), is adopted. A simple structural scheme is considered with the wall base completely constrained and the top side free.

Fig. 3(a) and (b) show the effect of the material parameters b_t and a_t on the wall generalized restoring force curve, considering for the others those quantities collected in Table 1 and setting $l_c = 500$ mm. The analyses are carried out by imposing a monotonically increasing horizontal displacement, s, to all nodes of the top free side. To be noted is that the b_t parameter affects the maximum load value, while the slope of the softening branch remains the same. Moreover, as b_t increases, the peak strength is reached at larger displacements (Fig. 3(a)). Instead, the a_t parameter mainly rules the post-peak behavior, with little influence on the maximum load value: as a_t reduces, more severe decreasing branches are obtained (Fig. 3(b)). However, in all cases, the panel response is characterized by strength and stiffness degradation due to the onset of a damaged zone at the wall base. As the structure is pushed towards the right, damage arises in the bottom left corner where the maximum tensile stresses are concentrated and, then, spreads out leading to a strongly damaged base section. As an example, Fig. 3(c) compares the tensile damage distribution at the imposed displacement $s = 9$ mm, for the three adopted values of a_t ($a_t = 0.99, a_t = 0.9$ and $a_t = 0.8$). More severe damage occurs for decreasing values of a_t due to the higher rate of evolution of the damaging mechanisms. Hence, the overall behavior strongly depends on the material tensile constitutive response which is, in turn, affected by the adopted value of a_t and b_t.

Looking at the cyclic response, which is more interesting for the scope of this study, significant characteristics of the masonry model emerge. Fig. 4(a) contains the generalized load–displacement loops obtained by imposing a cyclic displacement history with increasing amplitude at all nodes of the wall top side. Strength and stiffness degradation phenomena are clearly highlighted. The peak load is reached in the first cycle, then, the attained maximum force is gradually reduced in the subsequent cycles. Moreover, a significant stiffness variation is detected: as the amplitude of imposed displacement increases, damage grows leading to a reduction of the slopes of the unloading branches. However, a partial stiffness recovery occurs, near the axes origin, due to the opening and subsequent re-closing of the tensile cracks under reversal loading. Finally, plastic strains develop leading to hysteretic dissipation.

A further analysis is performed to better understand the cyclic response of the degrading structure model. A cyclic horizontal displacement, characterized by a firstly increasing, then constant, and finally decreasing amplitude, is applied at the wall top side. The response is shown in Fig. 4(b) focusing on the cycles obtained in correspondence to the same amplitude

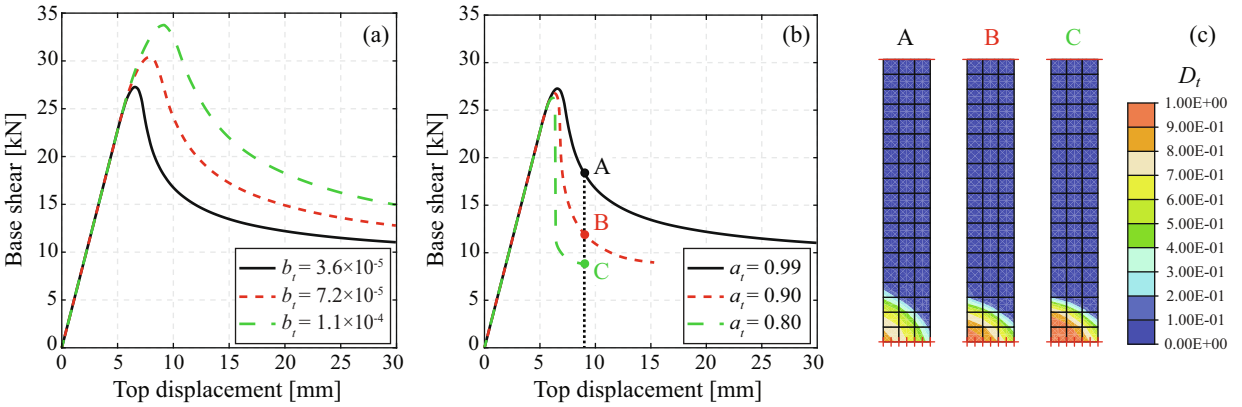

Fig. 3. Monotonic load–displacement response curve for different values of (a) b_t and (b) a_t; (c) distribution of the tensile damage D_t at point A, B and C of the global response curves.

Table 1
Material parameters adopted for the structure model.

Elastic parameters		*Plastic parameters*		*Damage parameters*				
E [MPa]	ν	σ_y[MPa]	H_k [MPa]	Y_{t0}	b_t	$a_t = a_c$	Y_{c0}	b_c
4000	0.2	1.5	0.7 E	5.2×10^{-5}	3.6×10^{-5}	0.99	1.3×10^{-4}	6×10^{-3}

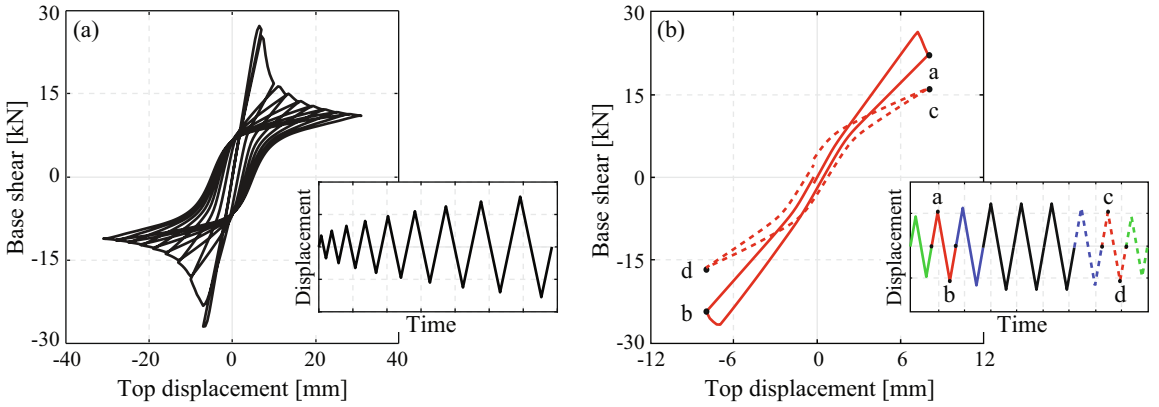

Fig. 4. Cyclic responses: (a) load–displacement curve obtained for imposed displacement with increasing amplitude and (b) response cycles obtained in correspondence of the same displacement amplitudes in a process where increasing and decreasing displacement amplitudes are imposed.

imposed at the beginning ('a-b' cycle) and end ('c-d' cycle) of the analysis. Although the structure moves between the same maximum displacements, the two cycles differ fully. This is due to the history-dependent characteristics of the adopted model. In fact, compared with the 'a-b' cycle, the structure reached higher displacements before achieving the 'c-d' cycle. During the loading history, the damage increases and modifies the strength and stiffness structural properties and, consequently, the shape of the restoring force loop. In fact, as a consequence of the degrading mechanism evolution, the reloading branch in the 'c-d' cycle shows a reduced slope, if compared with that of the 'a-b' cycle.

Summarizing, the history-dependent characteristic of the model strongly affects the static behavior of the structure but, even more so, the dynamic response, as analyzed in the following sections.

3. Model validation

The model presented in Section 2 is used to analyze the response of stiffness-strength degrading systems, such as masonry structural elements. In [22] some validation examples were provided to show the model ability to capture the cyclic quasi-static behavior of masonry panels, using experimental results available in literature for comparison. Here, the investigation is dynamic: the out-of-plane response of tuff masonry walls subjected to base accelerations is studied. First, the experimental tests performed at the Department of Structural and Geotechnical Engineering, Sapienza University of Rome, are described and, then, a comparison between numerical and experimental outcomes is discussed.

3.1. Experimental tests

Three tuff masonry walls, shown in Fig. 5, were tested under base harmonic acceleration histories on a uni-directional shaking table. The specimens were made of 19 courses of $370 \times 110 \times 260\,\text{mm}^3$ tuff bricks arranged in a running bond with 10 mm thick mortar joints, resulting in an overall size of: height $H = 2280$ mm, width $W = 570$ mm and thickness $t = 260$ mm. Panel dimensions were chosen according to the limits of the shaking table (in terms of maximum tolerable weight and range of working frequencies) and the geometry of masonry walls in real structures. Moreover, considering the weak level of anchorage on the top side, a common feature of masonry walls in historical buildings, a simple structural scheme was considered for the specimens: these were rigidly connected to the table at the base and free at the top, as shown in Fig. 5. Once each wall was placed on the shaking table, dynamic identification tests were performed to determine the natural frequencies of the flexural small amplitude vibrations associated to the out-of-plane modes. Fig. 6(a–c) show the Fourier spectra of each acceleration response (black lines) to the impacts of an instrumented hammer applied on the upper part of the panels and in the out-of-plane direction. The average curves are depicted with blue, red and green lines for the three samples, respectively called M1, M2 and M3 walls. Here, two resonance peaks occur in the range [0—80] Hz, representing the first, f_1, and second, f_2, natural frequencies of the out-of-plane flexural modes. It can be noted that, for M1 and M3 walls, the ratio f_2/f_1 confirms the fully constrained base condition and approaches the analytical value of 5.9 (evaluated by means

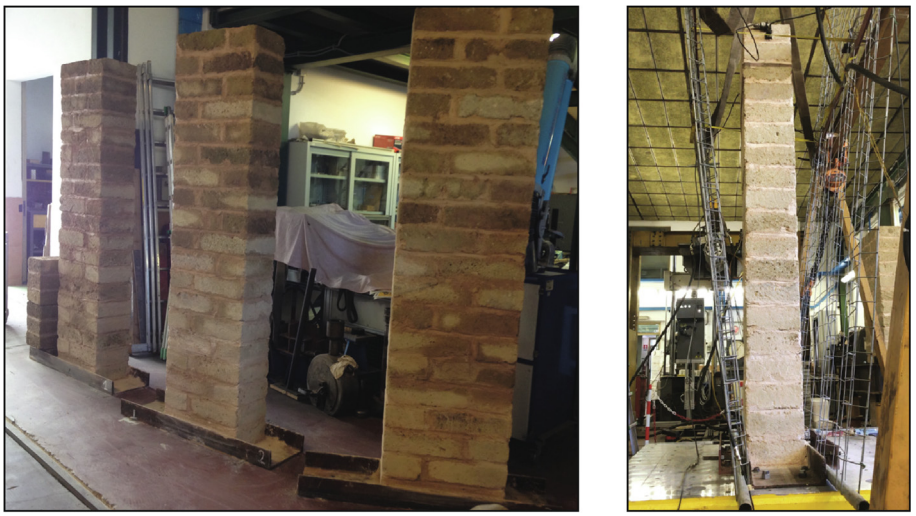

Fig. 5. Masonry tested specimens.

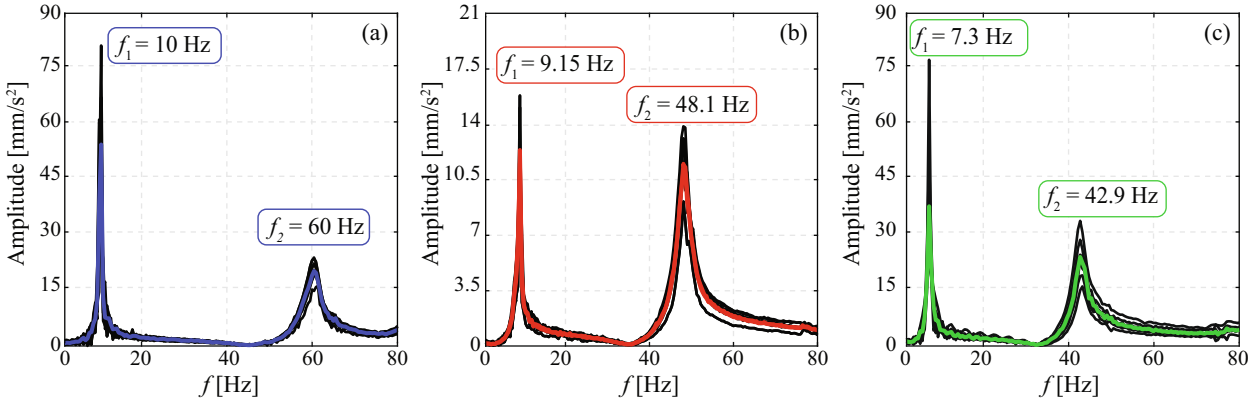

Fig. 6. Fourier spectra of the acceleration responses to the hammer impacts: (a) M1, (b) M2 and (c) M3 wall.

of the Timoshenko beam model). Conversely, a small discrepancy emerges between the analytical and experimental ratio f_2/f_1 for M2 wall, testifying an imperfect fixed constraint to the shaking table or defects introduced during the construction of the sample.

After performing the dynamic characterization through small amplitude vibration tests, the forced response of the walls was investigated by imposing sinusoidal base accelerations with different frequencies and amplitudes with the aim of analyzing the effects of degrading mechanisms on the dynamic amplification. Such simple input motions were selected to describe the dependency of the wall response on the main properties of the loading history (frequency and amplitude) in an effective and clear way and mainly to study the modification of *frcs* due to degradation. Hereafter, only the most relevant results are shown, which refer to an excitation frequency, Ω, lower than the first natural circular frequency, ω_1, such that $\Omega/\omega_1 = 0.65$. Table 2 contains the list of sinusoidal excitation amplitudes. For the higher amplitude tests (Run 2*b* - Run 5), the imposed time histories were characterized by incoming fade in cycle to avoid amplified transient responses. Moreover, small discrepancies between the target amplitudes contained in Table 2 and those actually imposed through the shaking table were detected, causing slightly larger excitation amplitudes, which have been taken into account in the numerical simulation.

Table 2
List of the input sinusoidal waves.

Run	1	2*a*	2*b*	3	4	5
Amplitude [mm/s²]	200	300	300	500	700	900

The response of the walls was measured by piezoelectric accelerometers and linear variable displacement transducers (LVDTs), located as shown in the outline of the experimental setup in Fig. 7. In detail, four LVDTs were placed in the upper part of the vertical sides of the panels, so as to detect any torsional motions, and one at the base of the shaking table to obtain results in terms of relative displacement.

As all samples exhibited the same phenomenological behavior, M3 wall is chosen as being representative to describe the masonry wall dynamic behavior. Fig. 8(a) shows the response, in terms of top relative displacement, arranged in sequence according to the input motions listed in Table 2. It emerges that the wall behavior was strongly affected by nonlinear degrading mechanisms evolving in the masonry, mainly due to a crack located in a mortar bed joint near the base, which in turn modified the structural natural frequency causing a variation of resonant conditions. As the excitation amplitude was increased and the damage evolved, the panel first frequency was reduced, thus approaching the driving frequency. During Run 3 a progressive slight amplification can be noted, followed by a steep growth, typical of the resonant conditions, in Run 4. Afterwards, a fairly stable response occurred, testifying that the panel has moved away from the resonant conditions. These considerations seem to be confirmed by the Fourier spectra of the responses shown in Fig. 8(b). For all runs, two dominant peaks appear: one at the driving frequency (4.75 Hz) and another at the first frequency of the structure. It is interesting to note how the peak of the first own frequency moved from the right to the left side of the input frequency, passing through resonance due to damaging phenomena.

Finally, it should be mentioned that, for input acceleration amplitudes higher than those analyzed here, a crack entirely crossed a mortar bed joint near the base leading to large oscillation responses characterized by the rocking motion of the wall. These results are collected and analyzed in [29], where an extensive experimental investigation of the free oscillation of a rigid body and a comparison with the analytical results is presented.

3.2. Experimental–numerical comparison

The described experimental outcomes are numerically reproduced by means of the model presented in the previous section. The material parameters used in the numerical simulation (Table 3) were set according to the available experimental data. In particular, Young's modulus, E, was determined through an inverse process on the basis of the wall natural frequencies and the material mass density, equal to $\rho = 1577\,\mathrm{kg/m^3}$, was determined by measuring the wall weight with a load cell. Regarding the strength properties, the compressive value (about 3 MPa) was derived from results of previous tests [30] performed on the same masonry material, whereas the tensile strength was set to fit the experimental outcomes.

The wall was discretized with (3×26) 9-node quadrilateral FEs, setting the nonlocal radius $l_c = 130\,\mathrm{mm}$. The FE equilibrium equations were obtained considering the lumped mass formulation and the Rayleigh damping factor equal to 3%. The Newmark time integration scheme was adopted, together with the Newton–Raphson procedure, to determine the nonlinear solution for each time step.

The comparison between numerical and experimental results, in terms of time history of the top displacement, is shown in Fig. 8(c). Overall a good agreement emerges, as the numerical model is able to capture the actual resonance and the max-

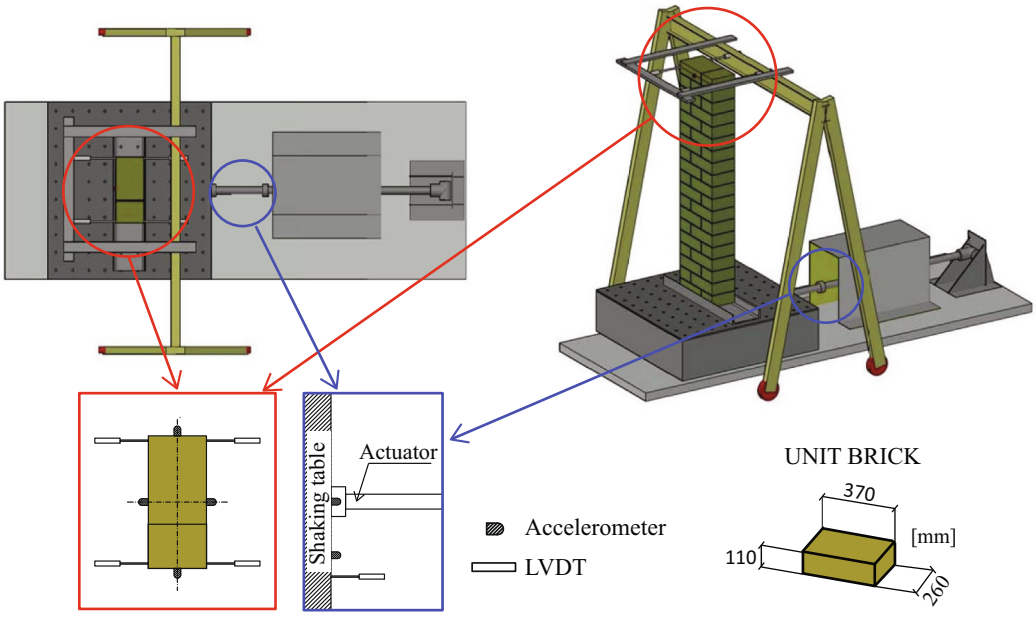

Fig. 7. Schematic of experimental setup.

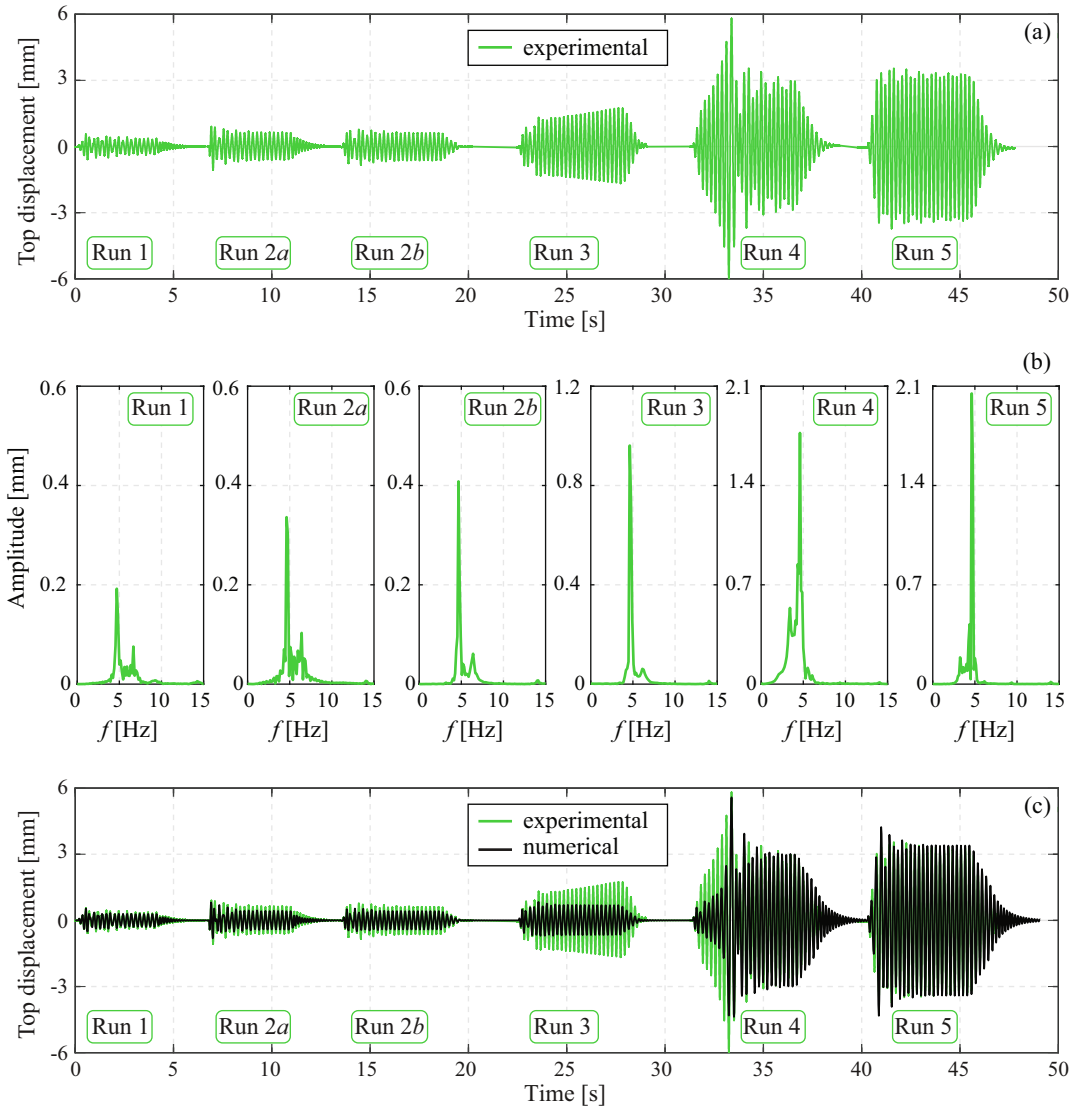

Fig. 8. M3 wall: (a) experimental top displacement response, (b) Fourier spectra of the experimental responses at each run, (c) comparison between experimental and numerical responses.

Table 3
Material parameters adopted for M3 wall.

Elastic parameters		Plastic parameters		Damage parameters				
E [MPa]	ν	σ_y [MPa]	H_k [MPa]	Y_{t0}	b_t	$a_t = a_c$	Y_{c0}	b_c
1300	0.18	3.7	0.1 E	1×10^{-5}	3.5×10^{-5}	0.995	1×10^{-3}	6×10^{-3}

imum displacement exhibited by the wall. In the first runs (1, 2a and 2b) a slight damage occurs and the experimental and numerical responses are well overlapped. Instead, some discrepancies emerge in Run 3: in the experimental test, degradation produces an increase of the structure deformability moving the natural frequency toward the driven one, totally absent in the numerical simulation. However, the differences between experimental and numerical results are limited to Run 3, as the transition through the resonance in both cases occurs during Run 4. Such a transition is more concentrated in the numerical description, as confirmed by the fast spread of damage at the base of the wall (not reported here). The situation remains stable during Run 5, without any increase in damage, with a good agreement between numerical and experimental displacement amplitudes.

4. Frequency response curves

The behavior of the structural model, analyzed in Section 2 under monotonic and cyclic static actions, is here studied considering the dynamic response. Firstly, the wall is subjected to sine-sweep type acceleration histories to evaluate its frequency response curves and highlight the damaging effects. Then, response to harmonic excitation with fixed frequency is considered to assess its correlation with the *frcs*.

4.1. Response to harmonic excitation with increasing and decreasing frequency

The base accelerations, $\ddot{u}_g = U\sin(\Omega(t)t)$, imposed to the cantilever masonry wall are characterized by linearly increasing and decreasing excitation frequency $\Omega(t)$, varying in the range $[0.2-1.5]$ of the first small amplitude natural frequency of the system $\omega_1 = 39.12\,\text{rad/s}$ ($f_1 = 6.23$ Hz), having set $\rho = 2000\,\text{kg/m}^3$. The other mechanical parameters are those contained in Table 1. In what follows, 'sweep 1' denotes the acceleration history with increasing driving frequency, 'sweep 2' with a decreasing one.

Fig. 9(a) and (b) contain the wall *frcs* evaluated for different values of the excitation intensity, that is $U/g = 0.04, 0.05, 0.06$ (g denotes the gravity acceleration), and with reference to sweep 1 and 2, respectively. The colored curves account for the material nonlinearity (i.e. damage and plasticity), the black curves refer to the elastic response (i.e. linear elastic constitutive law is assumed for the material), shown for the sake of comparison. All curves are derived by associating the response amplitude (in terms of relative displacement of the top central point P of the panel with respect to the base) to each excitation frequency and considering a damping Rayleigh ratio equal to 3%.

Looking at the response to sweep 1 (Fig. 9(a)), the *frcs* are characterized by narrow bells and peaks that slowly move towards lower values of Ω/ω_1, as the ratio U/g increases. These features are the consequence of degradation occurring in

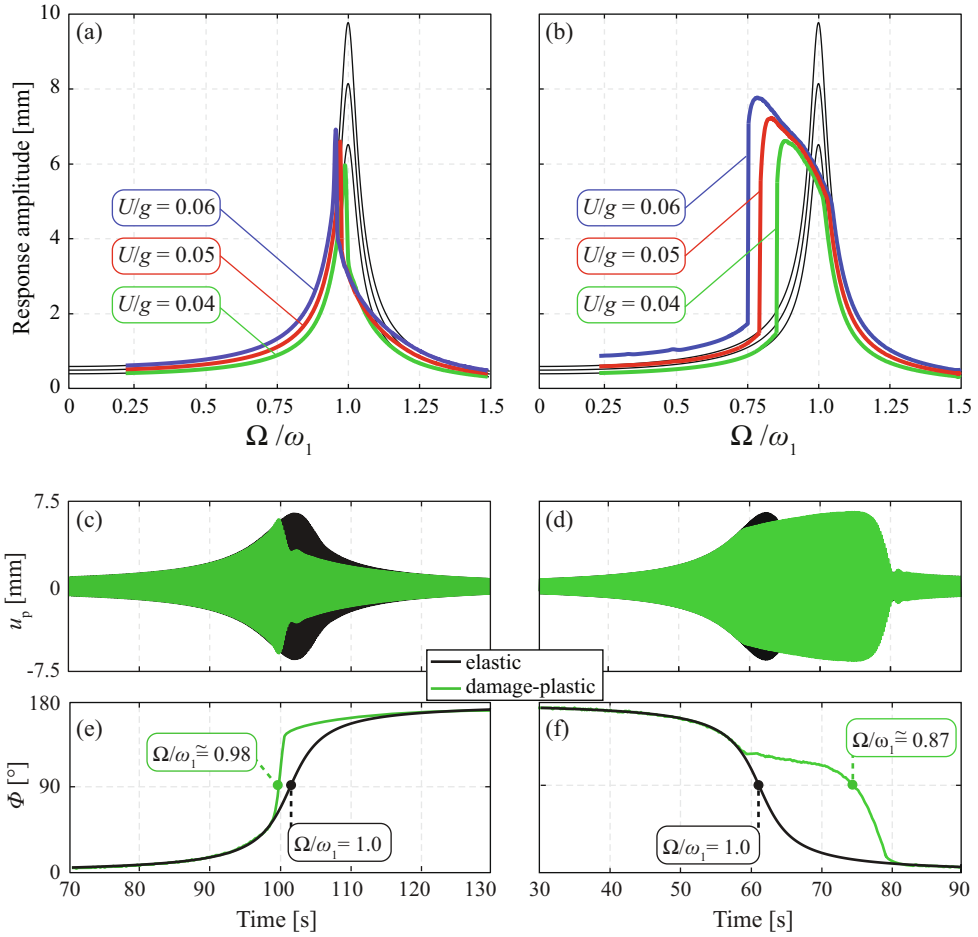

Fig. 9. Response to (a,c,e) sweep 1 and (b,d,f) sweep 2: (a,b) wall frequency response curves for different values of U/g (elastic response corresponds to black lines, damage-plastic response refers to colored lines), (c,d) time histories of the top relative displacement in linear elastic and damage-plastic cases, (e,f) time histories of the phase angle Φ for $U/g = 0.04$.

masonry material during the loading history. Indeed, as damage starts and evolves, the structural stiffness decreases, leading to a reduction of the first natural frequency, while the forcing frequency increases according to sweep 1 history. Due to the combination of these two conditions (i.e. increase of the forcing frequency and decrease of the natural frequency), the structure reaches the resonant condition for values Ω/ω_1 lower than unit, then quickly exits.

The described phenomenon can be better appreciated in Fig. 9(c) and (e), which refer to the case of $U/g = 0.04$, chosen as example. Focusing attention on the significant time interval of the loading history, Fig. 9(c) shows the response displacement of the monitored point *P* and Fig. 9(e) reports the variation of the phase angle Φ between the response and the input action, evaluated by means of the time delay. In both figures the green and black lines refer to the damage-plastic and elastic response, respectively. As expected, in the elastic case, the variation of the phase angle follows the quite smooth trend, typical of the damping Rayleigh factor considered, attaining the value $\Phi = 90^\circ$ when $\Omega/\omega_1 = 1$. Conversely, in the case of the damage-plastic response, a sudden inversion phase occurs around $\Omega/\omega_1 \cong 0.98$, pinpointing the fact that the structure quickly approaches and leaves the resonant condition. This snap transition through the resonance also justifies the low peak response obtained in the nonlinear case if compared with the elastic case (see Fig. 9(a) and (c)).

Quite different features emerge when sweep 2 is applied. In this instance, the *frcs* show that the resonant frequency markedly reduced as the value of U/g increased (Fig. 9(b)). This frequency at the peak response practically coincides with the system natural frequency and, clearly, depends on the forcing amplitude. The overall behavior is ruled, once again, by the variation of the wall frequency with respect to the driving one. However, unlike sweep 1, when the damaging mechanisms evolve, the natural frequency and the excitation frequency follow the same decreasing trend along the resonant branch. Consequently, the structure slowly approaches to the resonance condition and reaches the peak response at a time, and therefore at a frequency, very different with respect to the corresponding elastic value, as shown in Fig. 9(d) by the displacement time histories. This phenomenon can also be understood by analyzing the angle phase progression in Fig. 9(f). At the beginning of the loading history, the green and black curves, referring to the damage-plastic and elastic case respectively, are overlapped. Then, the two curves separate and, similarly to the sweep 1 case, achieve the inversion phase condition at different values of Ω/ω_1, but, now, the structure follows a longer path before attaining $\Phi = 90^\circ$.

Another significant characteristic emerges from *frcs* in Fig. 9(b): the peak response of the damaged structure is lower if compared to the corresponding elastic and the size of this gap depends on the forcing amplitude. This is due to the onset of plastic strains, which contribute to the dissipation process. As evident from Fig. 4(a), the width of the response cycles, and consequently the dissipated energy, increases with increasing displacement. Indeed, the response of the damaged structure can be larger with respect to the elastic if the plasticity effects are neglected, as observed in [22].

Summarizing, it is deduced that the response dynamic amplification is affected by the loading history, as typically occurs for nonlinear systems. However, differently from systems with a nonlinear invariant restoring force, the *frcs* for increasing and decreasing forcing frequency do not reconnect themselves. This is clearly proved in Fig. 10(a), where both the curves obtained with sweeps 1 and 2 for $U/g = 0.06$ are reported. It is evident that the *frc* for increasing frequency cannot overlap the resonant branch obtained for decreasing frequency. This is due to the irreversible effects of damage, which notably modify the restoring force loop (see Fig. 4(b)), making the equilibrium points strongly history dependent.

To make the concept even more explicit, it is useful to introduce a global damage variable and use it to relate the dynamic amplification to the structural damage state. The global tensile damage index D_t^g, defined according to [22,31], is determined as a weighted average on the damaged area at the end of the analysis, A_D, of the tensile damage variable, D_t, evaluated at each integration point of the FE model, as:

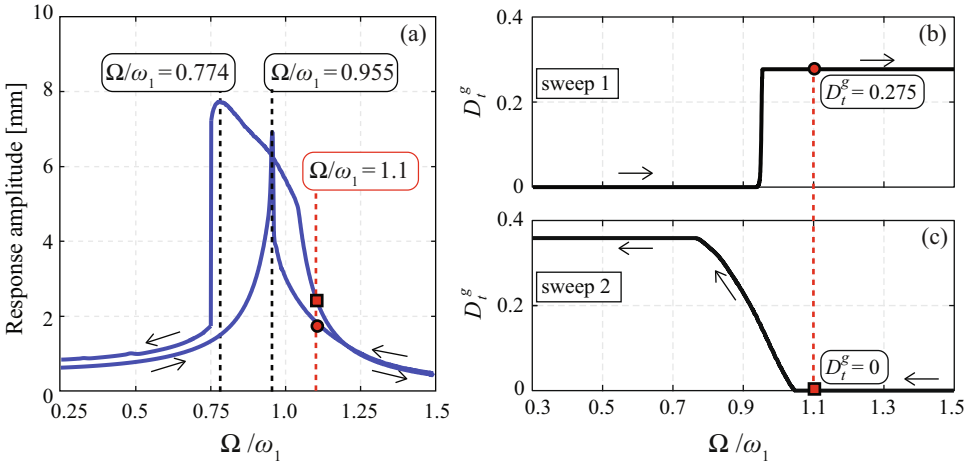

Fig. 10. Response to sweep 1 and 2 setting $U/g = 0.06$: (a) *frcs*, variation of the global damage index D_t^g with Ω/ω_1 for (b) sweep 1 and (c) sweep 2.

$$D_t^g = \frac{1}{A_D}\int_A D_t\, dA \tag{6}$$

Varying between 0 and 1, high values of D_t^g indicate a severe damage state. The adopted definition of D_t^g cannot provide information on the damage spatial distribution, but is a scalar measure of the damage severity. However, in this problem the quantity is particularly meaningful because damage localizes at the wall base, as a consequence of the cantilever scheme considered and the imposed excitation which mainly excites the first mode vibration. Thus, the different dynamic amplification obtained with the two sweeps can be clarified by the defined damage index. Let us focus on the ratio $\Omega/\omega_1 = 1.1$ in Fig. 10(a). The equilibrium points denoted with circle and square indicators represent the response obtained with sweep 1 and 2, respectively. Regarding sweep 1, the wall approaches to the ratio $\Omega/\omega_1 = 1.1$ with a damaged state quantified by a global damage value equal to 0.275 (Fig. 10(b)) due to the amplification experienced during the passage through resonance. Conversely, in the case of sweep 2, at $\Omega/\omega_1 = 1.1$, the wall is undamaged yet (Fig. 10(c)), with higher response amplification. This evidence seems to contradict the expected behavior that a damaged, and therefore more flexible, structure exhibits larger displacements than the undamaged one, under the same force intensity. However, the ratio between the forcing and natural frequencies plays a significant role on the dynamic response amplification. At $\Omega/\omega_1 = 1.1$ the previous histories of the oscillating wall are quite different, as documented by the damage indices. In particular, for sweep 2 the own frequency is still equal to the initial ω_1 value, whereas for sweep 1 the experienced damage strongly reduces the natural frequency and the effective frequency ratio is greater than 1.1 with a consequent lower dynamic amplification.

4.2. Response to harmonic excitation with fixed frequency

To enrich the dynamic characterization, the response to sinusoidal acceleration histories with a fixed frequency is investigated, assuming zero displacement and velocity initial conditions. The analyses are conducted setting $U/g = 0.06$ and imposing some incoming fade in cycle to avoid amplified transient solutions.

In Fig. 11(a) maximum and steady-state responses obtained for each loading history are denoted with circle and cross points, respectively. Such points are depicted together with the corresponding *frcs* with the aim of comparing the solutions.

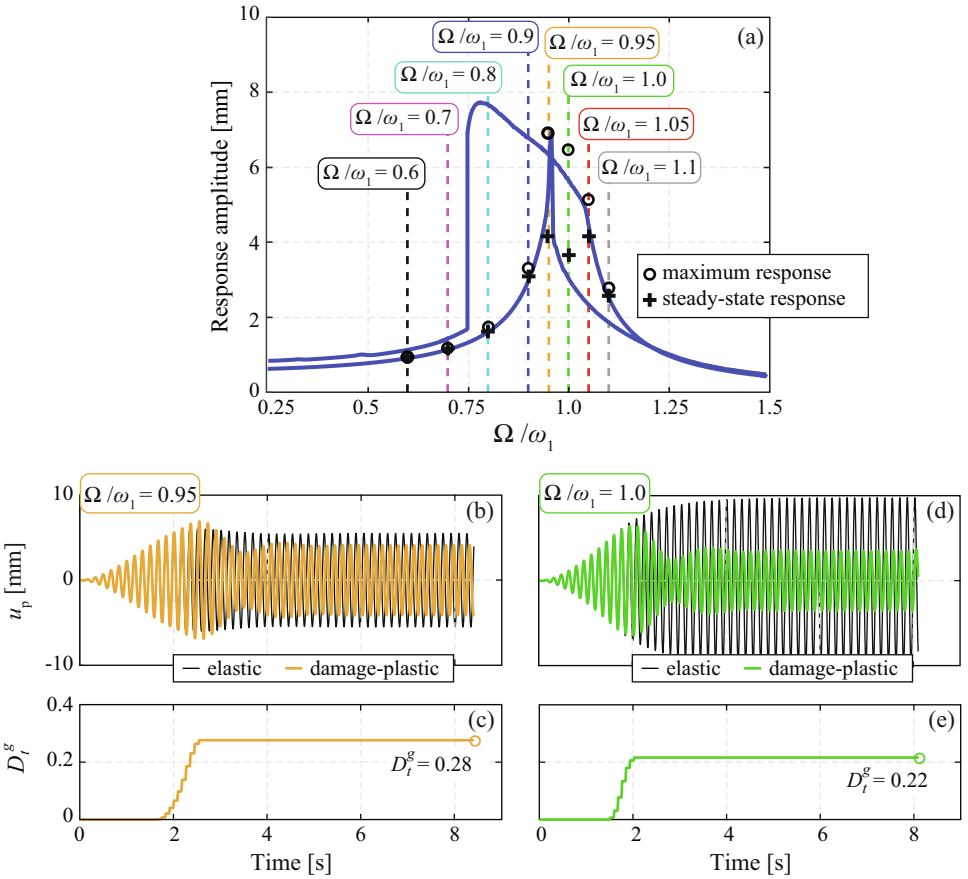

Fig. 11. Response to base sinusoidal accelerations with fixed driving frequency setting $U/g = 0.06$: (a) comparison between maximum and steady-state response with *frcs*, time histories of the (b,d) top displacement and of the (c,e) global damage index for Ω/ω_1 equal to 0.95 and 1.0, respectively.

It emerges that for the ratio Ω/ω_1 equal to 0.6, 0.7, 0.8 and 0.9, points denoting maximum and steady-state response at fixed forcing frequency are practically coincident and placed on the curve corresponding to sweep 1, due to null initial conditions. For these frequency ratios, no inelastic phenomena occur, neither for sweep 1 (see Fig. 10(b)) nor for a fixed frequency and, hence, the wall behaves as an elastic structure. A similar behavior occurs for the ratio Ω/ω_1 equal to 1.05 and 1.1, but now, the steady-state response at fixed driving frequency overlaps with that evaluated with sweep 2, as the histories experienced by the wall are very close.

More interesting comments can be made for the ratio Ω/ω_1 equal to 0.95 and 1.0, as a significant difference emerges between maximum response, steady-state response and equilibrium points of the *frcs*. Moreover, to better frame the phenomenon, it is also useful to refer to the elastic behavior. Fig. 11(b,d) compare the elastic responses (black lines) with the damage-plastic ones (colored lines). Obviously, the responses are overlapped until the nonlinear phenomena occur, as proved by the global damage index in Fig. 11(c,e) and, in both the nonlinear cases, maximum amplitude obtained in the initial phases is notably greater than the steady-state one. In the case of $\Omega/\omega_1 = 0.95$, the onset of damage causes reduction of the wall natural frequency so as to induce resonance. Moreover, if the variation of the phase angle Φ were to be plotted, the passage through the value 90° would be detected. In the case of $\Omega/\omega_1 = 1.0$, damaging mechanisms immediately cause a decrease of the response amplitude with respect to the elastic case, as the natural frequency of the damaged structure departs from the excitation frequency. However, points representative of the steady state response are not located on the resonant branch of the *frc* obtained with sweep 2, but these are closer to the curve corresponding to sweep 1. In fact, for this excitation amplitude and these frequencies, the wall exhibits about the same maximum top displacement and the same damage (see Figs. 10(b) and 11(c,e)), when excited with sweep 1 or with the fixed frequency harmonic load.

The analyses performed pinpointed that the onset and evolution of damaging mechanisms definitely modify the restoring force loops and, consequently, the response dynamic amplification. The *frcs* show, similarly to those of systems with reduced hysteresis [32,33], multi-valued characteristic. However, even limiting attention to the stable solutions reached during sweeps 1 and 2, not unique curves are obtained and the region of coexisting solutions is quite large around the initial wall frequency, as a consequence of the irreversible effects of damage which makes the equilibrium points strongly history dependent. It can be remarked that if damage was neglected, reducing the structure to an elasto-plastic system, all these phenomena would disappear and single-valued *frcs* would be obtained, according to the consolidated results found in [33] for systems with full hysteresis.

5. Conclusions

The dynamic response of a linear mechanical system is exhaustively described by the frequency response function, which is uniquely related to its dynamic parameters. The scenario is quite different for nonlinear systems, also because nonlinearity implies a wide variety of restoring forces which describe geometrical, piece-wise and material nonlinear behaviors. Many studies have investigated the role of the *frc*, and its backbone, in representing and predicting the response of nonlinear systems. However, the literature on nonlinear dynamics usually refers to restoring forces which are invariant with respect to the deformation history because damage is not considered. Behavior of systems affected by material nonlinearities, which are very sensitive to damaging effects of repeated loads, has been studied only under specific excitations, generally nonstationary, such as earthquakes, wind, blast and other.

In a previous paper [22] the authors adopted a nonlinear constitutive model, accounting for damage and plastic phenomena, to describe the static and dynamic response of a simple structure, a masonry cantilever wall. This latter is taken here as a suitable example of a real system with decay to be used in the investigation of the modification of *frcs* due to damaging phenomena.

First, experimental shaking table tests are developed to validate the finite element model of the masonry wall and prove its capability in correctly describing both the variation of the dynamic characteristics caused by increasing intensity of harmonic excitation, and the occurring resonance. Then, an analysis of the *frcs* is explored. The curves depend on the level of external loading, typical of any nonlinear system, but now, another fundamental characteristic of the invariant systems is lost, that is the frequency response curves obtained with increasing and decreasing driven frequency do not coincide. Indeed, the two *frcs* are quite different in a wide region around the resonance. For increasing external frequency, the non-resonant branch of stable solutions continues up to the resonance frequency, which is close to the initial wall frequency, because no damage so far occurs. At resonance, a sharp increment of the response, and consequently of the damage, reduces the own frequency of the structure, which immediately goes out from the resonance, and the response curve tends to zero. This *frc* shows a clearly defined peak, with a shape similar to that of linear systems. Completely different is the *frc* obtained from decreasing driven frequency: in this case the response smoothly increases and the damage produces a reduction of the own frequency, which remains close to the external one on the resonant branch up to peak resonance, attained at a frequency much lower than the initial value. Moreover, the two *frcs* described exhibit two different periodic solutions for each frequency, depending on the history experienced before reaching the equilibrium point. It has also been shown that the response to harmonic excitations with fixed frequency and null initial conditions gives other solutions with quite different maximum and steady-state responses, generally placed between the two previous ones. Evidence of the not unique information associated with the *frc*, which is definitely dependent upon the deformation history, is given.

In conclusion, degradation phenomena induced by the dynamic process seem to destroy the signature of frequency response curves. Novel perspectives are needed to understand the information that can be deduced from a *frc* to define the dynamic properties of a system and predict its forced response. It goes without saying that the not uniqueness of the *frcs* depending on the deformation history requires further investigation with different categories of loading, such as quasi-periodic, non-stationary, random and impulsive, to ascertain other signatures to add to the *frcs* in view of better characterization of the dynamic behavior of degrading structures.

CRediT authorship contribution statement

C. Gatta: Methodology, Formal analysis, Software, Investigation, Writing - original draft. **F. Vestroni:** Conceptualization, Investigation, Supervision, Writing - review & editing. **D. Addessi:** Methodology, Supervision, Writing - review & editing.

Declaration of Competing Interest

The authors declare that they have no known competing financial interests or personal relationships that could have appeared to influence the work reported in this paper.

Acknowledgments

The support of Italian MIUR (Minister of Education University and Research) under the grant PRIN-2015 2015TTJN95, P.I. Fabrizio Vestroni, 'Identification and monitoring of complex structural systems' is gratefully acknowledged.

References

[1] H. Elizalde, M. Imregun, An explicit frequency response function formulation for multi-degree-of-freedom non-linear systems, Mech. Syst. Signal Process. 20 (8) (2006) 1867–1882.
[2] Z.K. Peng, Z.Q. Lang, S.A. Billings, Linear parameter estimation for multi-degree-of-freedom nonlinear systems using nonlinear output frequency-response functions, Mech. Syst. Signal Process. 21 (8) (2007) 3108–3122.
[3] Z.K. Peng, Z.Q. Lang, S.A. Billings, Nonlinear parameter estimation for multi-degree-of-freedom nonlinear systems using nonlinear output frequency-response functions, Mech. Syst. Signal Process. 22 (7) (2008) 1582–1594.
[4] X. Wang, G.T. Zheng, Equivalent Dynamic Stiffness Mapping technique for identifying nonlinear structural elements from frequency response functions, Mech. Syst. Signal Process. 68 (2016) 394–415.
[5] X. Wang, T.L. Hill, S.A. Neild, Frequency response expansion strategy for nonlinear structures, Mech. Syst. Signal Process. 116 (2019) 505–529.
[6] A. Carrella, D.J. Ewins, Identifying and quantifying structural nonlinearities in engineering applications from measured frequency response functions, Mech. Syst. Signal Process. 25 (3) (2011) 1011–1027.
[7] S. Peter, M. Scheel, M. Krack, R.I. Leine, Synthesis of nonlinear frequency responses with experimentally extracted nonlinear modes, Mech. Syst. Signal Process. 101 (2018) 498–515.
[8] G. Zhang, C. Zang, M.I. Friswell, Measurement of multivalued response curves of a strongly nonlinear system by exploiting exciter dynamics, Mech. Syst. Signal Process. 140 (2020) 106474.
[9] W. Lacarbonara, F. Vestroni, Nonclassical responses of oscillators with hysteresis, Nonlinear Dyn. 32 (3) (2003) 235–258.
[10] P. Casini, F. Vestroni, Nonlinear resonances of hysteretic oscillators, Acta Mech. 229 (2) (2018) 939–952.
[11] D. Capecchi, F. Vestroni, Steady-state dynamic analysis of hysteretic systems, J. Eng. Mech. 111 (12) (1985) 1515–1531.
[12] D. Bernardini, G. Rega, Evaluation of different SMA models performances in the nonlinear dynamics of pseudoelastic oscillators via a comprehensive modeling framework, Int. J. Mech. Sci. 130 (2017) 458–475.
[13] M. Ismail, F. Ikhouane, J. Rodellar, The hysteresis Bouc-Wen model, a survey, Arch. Comput. Meth. Eng. 16 (2) (2009) 161–188.
[14] B. Carboni, W. Lacarbonara, Dynamic response of nonlinear oscillators with hysteresis, in: International Design Engineering Technical Conferences and Computers and Information in Engineering Conference, American Society of Mechanical Engineers, 2015.
[15] J. Awrejcewicz, L. Dzyubak, C.H. Lamarque, Modelling of hysteresis using Masing–Bouc-Wen's framework and search of conditions for the chaotic responses, Commun. Nonlinear Sci. Numer. Simul. 13 (5) (2008) 939–958.
[16] G. Gatti, M.J. Brennan, Inner detached frequency response curves: an experimental study, J. Sound Vib. 396 (2017) 246–254.
[17] A. Cammarano, T.L. Hill, S.A. Neild, D.J. Wagg, Bifurcations of backbone curves for systems of coupled nonlinear two mass oscillator, Nonlinear Dyn. 77 (2014) 311–320.
[18] D.J. Wagg, Understanding the dynamics of multi-degree-of-freedom nonlinear systems using backbone curves, Procedia Eng. 199 (2017) 78–85.
[19] A.K. Kottari, A.E. Charalampakis, V.K. Koumousis, A consistent degrading Bouc-Wen model, Eng. Struct. 60 (2014) 235–240.
[20] D. Liberatore, D. Addessi, M. Sangirardi, An enriched Bouc-Wen model with damage, Eur. J. Mech.-A/Solids 77 (2019) 103771.
[21] D. Addessi, C. Gatta, F. Vestroni, Dynamic response of a damaging masonry wall, Procedia Eng. 199 (2017) 152–157.
[22] C. Gatta, D. Addessi, F. Vestroni, Static and dynamic nonlinear response of masonry walls, Int. J. Solids Struct. 155 (2018) 291–303.
[23] A.M. D'Altri, V. Sarhosis, G. Milani, J. Rots, S. Cattari, S. Lagomarsino, E. Sacco, A. Tralli, G. Castellazzi, S. de Miranda, Modeling strategies for the computational analysis of unreinforced masonry structures: review and classification, Arch. Comput. Meth. Eng. (2019) 1–33.
[24] M. Cervera, C. Tesei, G. Ventura, Cracking of quasi-brittle structures under monotonic and cyclic loadings: a d+/d- damage model with stiffness recovery in shear, Int. J. Solids Struct. 135 (2018) 148–171.
[25] P. Di Re, D. Addessi, A mixed 3D corotational beam with cross-section warping for the analysis of damaging structures under large displacements, Meccanica 53 (6) (2018) 1313–1332.
[26] J.C. Simo, R.L. Taylor, A return mapping algorithm for plane stress elastoplasticity, Int. J. Numer. Meth. Eng. 22 (3) (1986) 649–670.
[27] R.L. Taylor, FEAP-A finite element analysis program. Version 8.5, in: Department of Civil and Environmental Engineering, University of California at Berkeley, California, 2017.
[28] G. Pijaudier-Cabot, Z.P. Bažant, Nonlocal damage theory, J. Eng. Mech. 113 (10) (1987) 1512–1533.
[29] E. Cappelli, A. Di Egidio, F. Vestroni, Analytical and experimental investigation of the behavior of a rocking masonry tuff wall, J. Eng. Mech. 146 (6) (2020) 04020048.

[30] G. Marcari, M. Basili, F. Vestroni, Experimental investigation of tuff masonry panels reinforced with surface bonded basalt textile-reinforced mortar, Compos. Part B: Eng. 108 (2017) 131–142.
[31] J. Toti, V. Gattulli, E. Sacco, Nonlocal damage propagation in the dynamics of masonry elements, Comput. Struct. 152 (2015) 215–227.
[32] W.D. Iwan, The steady-state response of the double bilinear hysteretic model, J. Appl. Mech. (1965) 921–925.
[33] D. Capecchi, F. Vestroni, Periodic response of a class of hysteretic oscillators, Int. J. Non-Linear Mech. 25 (2–3) (1990) 309–317.